Thermal Effects on Propagation in Polymer Waveguides in Optical Interconnects

التأثيرات الحرارية على الانتشار في الدلائل الموجية المصنعة من البوليمر في الوصلات الضوئية

Atef M. Rashed

Department of Electrical Engineering, Aston University,

27 Fieldhead Road, Birmingham B11 3PS, United Kingdom

ملخص

تحسب نمذجة الفرق المنتهى لانتشار الشعاع تأثير المنحدرات الحرارية فى المسطحات الخلفية الضوئية على انتشار المجال الضوئى في الدلائل الموجية المسحوبة خطيا والمتعددة الحالات والمصنوعة من البوليمرات. بالمقارنة مع الدلائل الموجية المستقيمة فإن المداخل المسحوبة تعطى اشتباكا محسنا للقدرة لنطاق عريض من التزحزح العرضي للمصادر الضوئية. تقلل المنحدرات الحرارية السطحية بقيمة 0.5 د/ميكرون من هذه الميزة بسبب التأثير الضوئى الحرارى فى البوليمر. وعلى أى حال فإن المنحدرات الحرارية السطحية الأكبر من ذلك تحسن من اشتباك القدرة فى نطاقين منفصلين من التزحزح العرضي للمصادر الضوئية.

ABSTRACT

Finite difference beam propagation modelling (FD-BPM) calculates the effect of thermal gradients in an optical backplane on the optical field propagation in a polymer multimode linearly tapered waveguide. Compared to straight waveguides, tapered entrances offer improved power coupling for a wide range of optical source lateral offsets. Surface temperature gradients of 0.5 °C/μm across the taper were found to degrade this benefit due to the thermo-optic effect of the polymer. However, higher surface temperature gradients improve power coupling in two discrete ranges of lateral source offset.

1. INTRODUCTION

Large electronic systems are generally constructed as racks of many dismountable printed circuit board (PCB) cards. These boards, often known as daughter cards, are plugged into a much larger PCB at the back of the rack, known as the motherboard or backplane. The backplane supplies power to the daughter cards and has data buses to interconnect the daughter cards at high data rates using multilayer copper tracks. Data rates on the backplane are now reaching 10 Gb/s [1]. At this data rate copper tracks can only be used over short distances and this requires complex signal shaping to overcome attenuation and distortion due to high frequency parasitics and limited bandwidths [1]. Optical polymer waveguides integrated with a copper layer onto the FR4 PCB offer a low cost and compact approach to overcome the limitations of copper track interconnects alone [2, 3]. Resistive power tracks generate heat and electronic components mounted on the backplane also generate heat and transfer it via their leads to the backplane [4, 5]. The transferred heat and the existing air cooling system [6, 7] create thermal gradients across the polymer waveguide layers perturbing their refractive indices due to the thermo-optic (TO) effect [8]. Polymers with a low thermal conductivity, K and large temperature coefficient of refractive index, dn/dT exhibit greater temperature dependence [9] and consequently have a greater effect on the propagating optical field. The backplane is difficult to remove in the event of failure, so to improve the speed of servicing some of the active components are removed from the backplane and located on the daughter card that can easily be replaced. This includes the mounting of the laser and the photodetectors (PD) on the daughter cards. It may not be practical to remove all of the active components from the backplane and those remaining will generate thermal gradients. Optical sources and detectors may be misaligned relative to the waveguide when the daughter boards are inserted into the rack. To avoid the cost of precisely aligning optical connectors the waveguide should be designed to provide high source coupling efficiency even when offset [10]. This can be achieved using laterally tapered input waveguides [11]. In this paper we use FD-BPM [12] to investigate the effects of thermal gradients in the optical backplane on the optical field propagation in polymer multimode tapered waveguide and on the output power when the source is laterally offset [11].

2. WAVEGUIDE STRUCTURE AND GEOMETRY

In this paper we model a polymer multimode waveguide, Fig. 1 with a core refractive index, $n = 1.525$, a 0.5% step index profile between core and cladding and a core thickness of 25 μm. The thickness of each of the lower and upper cladding layers is 20 μm. The material loss is 0.03 dB/cm at the operating wavelength, $\lambda = 850$ nm. For core and both cladding layers the thermal conductivity, K is 0.18 W/(m.°C) and the temperature coefficient of refractive index, dn/dT is -0.0003 °C^{-1} [13]. The waveguide consists of a wide multimode input section that tapers down linearly in width over 1 mm from a width of 112 to 25 μm with a half taper-angle, $\varphi = 2.5°$. This section is followed by a straight multimode waveguide section, Fig. 1 (a), of 25 μm width and 1 mm length. Since the computational overhead can be prohibitive for simulating actual waveguide lengths of up to 50 cm we use a shorter total waveguide length of 2 mm in our simulation, which is still sufficient to illustrate the behaviour under investigation. The particular geometry chosen for simulation provides good tolerance for both

VCSEL and PD [14]. The thermal gradient is simulated by the inclusion of constant temperature, isothermal, elements on the top of the upper cladding layer and a continuous constant temperature, isothermal, reference layer at the bottom of the lower cladding layer. The elements are in the form of very thin stripes each of width W_h and relative temperature ΔT with respect to the bottom of the lower cladding layer. The constant temperature elements run along the waveguide longitudinal z-axis from the waveguide input aperture where $z = 0$ for a length of L_h. Fig. 1 (a) shows the top view of the waveguide with 5 constant temperature elements each of $W_h = 15$ μm and $L_h = 1$ mm and Fig. 1 (b) shows a schematic cross section of this configuration with the axes of the coordinate system used. For clarity a conventional right handed set of axes has not been used in our description. By changing W_h, L_h, the number of constant temperature elements and the x-coordinate of each constant temperature element specific thermal gradients can be realised.

In 10 Gb/s optical backplanes 10 Gb/s VCSELs of about 10 μm aperture may be used as optical sources [1]. In our model we chose a VCSEL emitting at its fundamental mode as the input source. The neglect of the higher order modes that cause larger divergence means that our analysis is only valid for small signal operation when the lowest order mode is likely to predominate. The input optical field used in the simulation, shown schematically in Fig. 1 (c), is a TE-polarised optical field with a Gaussian intensity profile of 10 μm width at e^{-1}. In this simulation we launched the input field into the waveguide structure along the z optical axis. Perfect source alignment corresponds to (0,12.5,0) launching position at the centre of the waveguide input aperture. In this paper we limit the
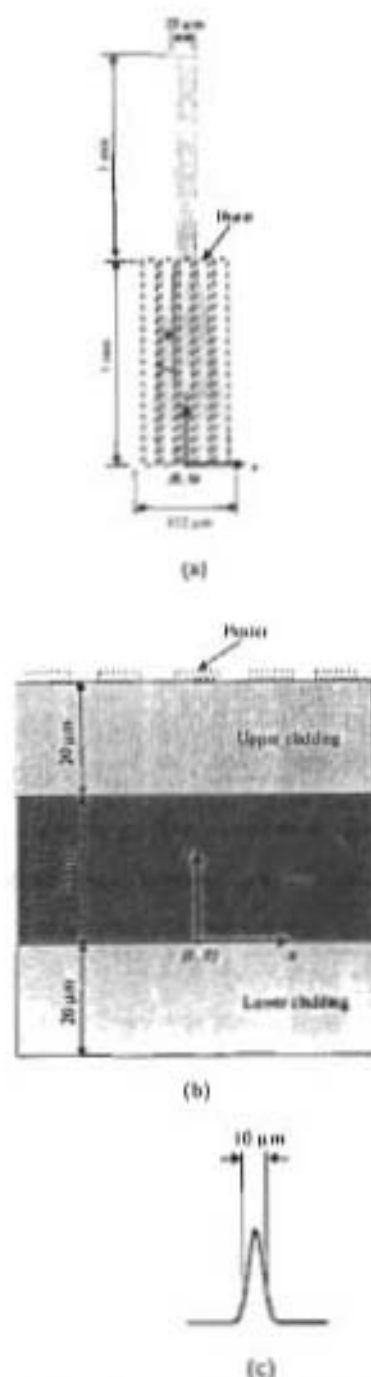

(a)

(b)

(c)

Fig. 1 (a) Top view of tapered waveguide with constant
temperature elements, heaters

(b) Schematic cross section of waveguide

(c) Schematic of the input optical field

investigations of the effects of the thermal gradients to the cases where the VCSEL is aligned or laterally offset with nonzero x-coordinate, $y = 12.5$ and assuming no angular misalignment.

3. NUMERICAL SIMULATION

The mathematical model used in the simulations is based on three-dimensional semi-vectorial FD-BPM (3D SV FD-BPM). This method employs the semi-vectorial wave equation for the field u [15]:

$$\frac{\partial u_x}{\partial z} = \frac{i}{2k}\left\{\frac{\partial}{\partial x}\left[\frac{1}{n^2}\frac{\partial}{\partial x}\left(n^2 u_x\right)\right] + \frac{\partial^2}{\partial y^2}u_x + \left(k^2 - \bar{k}^2\right)u_x\right\} \quad (1.\,a)$$

$$\frac{\partial u_y}{\partial z} = \frac{i}{2k}\left\{\frac{\partial}{\partial y}\left[\frac{1}{n^2}\frac{\partial}{\partial y}\left(n^2 u_y\right)\right] + \frac{\partial^2}{\partial x^2}u_y + \left(k^2 - \bar{k}^2\right)u_y\right\} \quad (1.\,b)$$

where x, y and z are the coordinates corresponding to the lateral, transverse and propagation directions, respectively. $\bar{k}$ is the reference wavenumber and $k = (2\pi/\lambda)\,n(x, y, z)$ is the spatially dependent wavenumber. Since the waveguide structure supports multimode propagation the wide-angle form of SV FD-BPM incorporating the Padé approximation is employed to overcome the paraxial nature of the wave equation [16, 17]. The Padé (1, 0) approximant has been used and transparent boundary conditions (TBC) [18] were implemented in the calculations to eliminate spurious reflections at the edges of the computation domain [19]. The temperature distribution inside the waveguide layers due to the constant temperature elements is determined by solving Poisson's equation [20]:

$$-\nabla\left(K(x,y,z)\nabla T(x,y,z)\right) = Q(x,y,z) \qquad (2)$$

where $T(x,y,z)$ is the temperature and $Q(x,y,z)$ is the heat generated per unit volume within the waveguide layers. For simplicity, we assumed constant thermal conductivity, K and used boundary conditions of isothermal surface heating elements and an isothermal reference temperature plane at $y = -20$ [20]. The calculated temperature distribution is used to determine the spatial perturbation of the refractive index in the structure through the temperature coefficient of refraction, dn/dT of the material. This perturbation is then incorporated into Eq. 1, which is solved by using FD-BPM. A mesh with step sizes of $\Delta x = \Delta y = 0.3$ μm and $\Delta z = 5$ μm is created within the waveguide structure and the wave equation is then integrated forward in z by replacing the partial derivatives with their finite difference approximations [21]. The optical field is successively calculated at each longitudinal step, Δz until reaching the end of the waveguide structure. The total power within the waveguide at the output aperture is then determined by computing the integral of the power in the calculated field at the corresponding z-position over the waveguide cross sectional area.

4. RESULTS

Fig. 2 (a) shows an example of the distribution of propagating optical power in the waveguide as a series of contours with zero source lateral offset and no heat applied, obtained by solving the wave equation. Fig. 2 (b) is the same as Fig. 2 (a) but with source laterally offset to $x = +50$ μm. Fig. 2 (c) is the same as Fig. 2 (b) but with heat applied to 5 constant temperature elements each with $W_h = 15$ μm and $L_h = 1$ mm. The constant temperature elements are centred at $x = -40$, -20, 0, 20 and 40 μm with $\Delta T = 80$, 80, 50, 20 and 20 °C, respectively. This temperature range lies within the

(a)

(b)

(c)
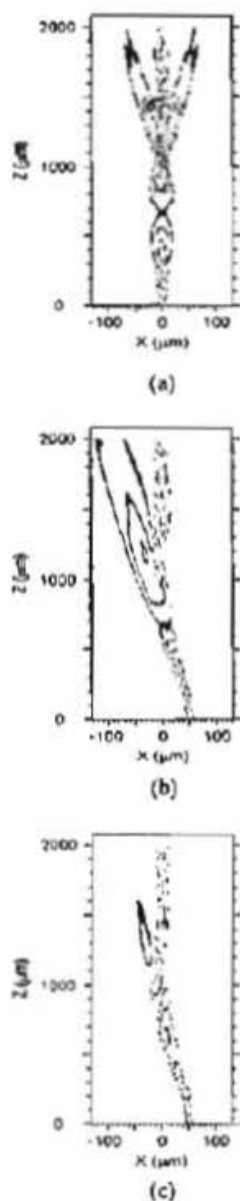
Fig. 2. Propagation of input field

(a) Source with zero offset and no heat applied

(b) Source with +50 μm offset and no heat applied

(c) Source with +50 μm offset and five constant
temperature elements with W_h =15 μm, L_u=1 mm
centred at x = -40, -20, 0, 20 and 40 μm with ΔT =
80, 80, 50, 20 and 20 °C, respectively

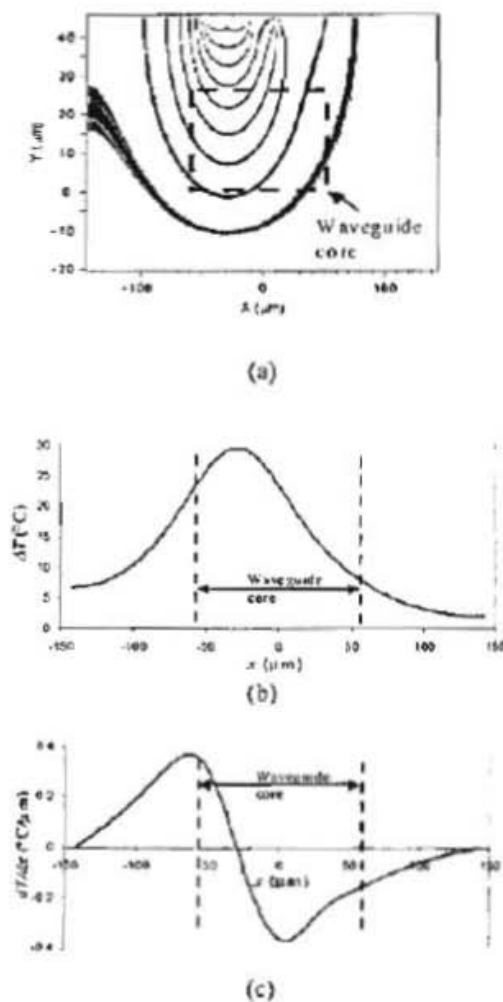possible range of operating temperature of many optical
backplane applications [22].

(a)

(b)

(c)

Fig. 3 (a) Temperature distribution across waveguide
layers at z = 0 due to five 15 μm wide, 1 mm
long constant temperature elements centred
at x = -40, -20, 0, 20 and 40 μm with ΔT =
80, 80, 50, 20 and 20 °C, respectively

(b) Corresponding temperature rise at y = +12.5
μm and z = 0 μm

(c) Corresponding thermal gradient at y = +12.5
μm and z = 0 μm

Indeed, this paper highlights the consequences of such heat pattern on the abovementioned waveguide as a guiding tool in the design process of the optical backplane. Fig. 3 (a) shows the contour lines of temperature distribution in a waveguide cross section at $z = 0$ due to 5 constant temperature elements each with $W_h = 15$ μm and $L_h = 1$ mm and centred at $x = -40, -20, 0, 20$ μm and 40 with $\Delta T = 80, 80, 50, 20$ and 20 °C, respectively. Fig. 3 (b) shows the corresponding relative temperature rise ΔT across the waveguide centre at $y = 12.5$ μm. Fig. 3 (c) shows the corresponding thermal gradient obtained by calculating the first derivative of the thermal distribution with respect to the lateral x-direction at the waveguide centre, $y = 12.5$ μm and $z = 0$. To investigate the effect of thermal gradients on source lateral misalignment several simulations were carried out with and without applied heat, each with the source at a different lateral offset along the x-axis. The output power normalised to the input power is plotted versus the source lateral offset with no heat applied in Fig. 4 (a). Fig. 4 (b) is the corresponding case with 5 constant temperature elements each with $W_h = 15$ μm and $L_h = 1$ mm and centred at $x = -40, -20, 0, 20$ and 40 μm with $\Delta T = 80, 80, 50, 20$ and 20 °C, respectively. In both figures the output power is calculated at each source position where zero output power is expected when the source is at ± 60 μm, completely off the input aperture which extends from -56 to +56 μm. Fig. 5 shows the contour lines of the normalised output power versus the source lateral offset and different constant temperature element lengths ranging from 0 where there is no heat applied to 2 mm covering the entire waveguide length. The number of constant temperature elements used is 5 each with $W_h = 15$ μm and centred at $x = -40, -20, 0, 20$ and 40 μm with $\Delta T = 80, 80, 50, 20$ and 20 °C, respectively.

These constant temperature elements created a thermal gradient of 1.5 °C/μm at the top of the upper cladding layer, $y = +45$ μm. A range of different thermal gradients at $y = +45$ μm was created by applying different temperature patterns to the same constant temperature elements at the same lateral positions with $L_h = 1$ mm. The ΔT patterns (°C) applied from left to right are [80,80,70,60,60], [80,80,60,40,40], [80,80,50,20,20] and [80,80,40,0,0].
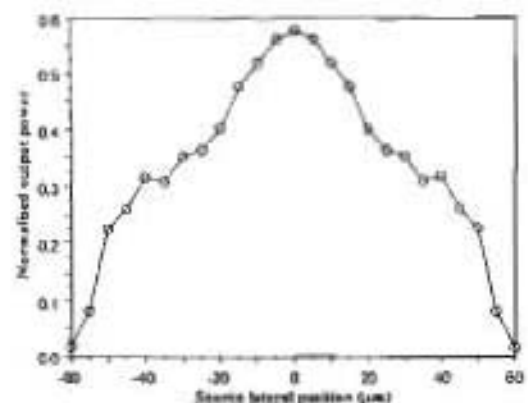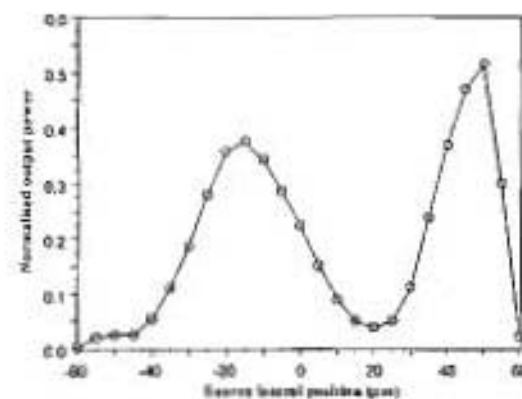
Fig. 4. Output power versus source lateral position
(a) No heat applied
(b) Heated with five 15 μm wide, 1 mm long constant temperature elements centred at $x = -40, -20, 0, 20$ and 40 μm with $\Delta T = 80, 80, 50, 20$ and 20 °C, respectively

These temperature patterns provide thermal gradients ranging from 0 to 2 °C/μm at y = 45. Zero thermal gradient is the case where is no heat applied. Fig. 6 shows the contour lines of the normalised output power versus the source lateral offset and different thermal gradients at y = +45 μm with L_b = 1 mm and the same parameters mentioned above.

To further investigate the heating effects higher surface thermal gradients need to be created without exceeding the operating temperature range. Therefore, 4 constant temperature elements each with W_b = 5 μm and L_b = 1 mm and centred at x = -20, -10, 10 and 20 μm are used. The ΔT patterns (°C) applied from left to right are [80,80,70,70], [80,80,60,60], [80,80,50,50], [80,80,40,40], [80,80,30,30], [80,80,20,20], [80,80,10,10] and [80,80,0,0]. These temperature patterns provide thermal gradients from 0 to 4 °C/μm at y = +45 μm. Zero thermal gradient is the case where is no heat applied.
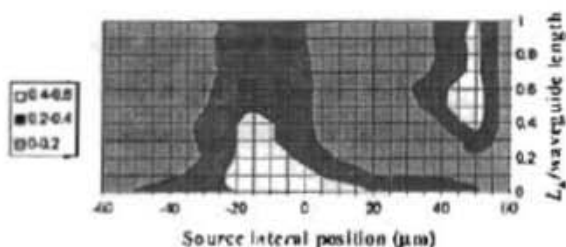

Fig. 5. Normalised output power versus source offset and ratio of constant temperature element length to waveguide length at surface $|dT/dx|$ of 1.5 °C/μm

Fig. 7 shows the contour lines of the normalised output power versus source lateral offset for different thermal gradients at y = +45 μm with 4 constant temperature elements each with W_b = 5 μm and L_b = 1 mm.
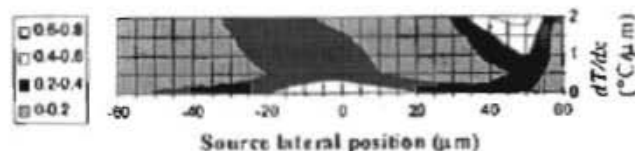

Fig. 6. Normalised output power versus source offset and surface $|dT/dx|$ with 5 constant temperature elements, W_b = 15 μm and L_b = 1 mm
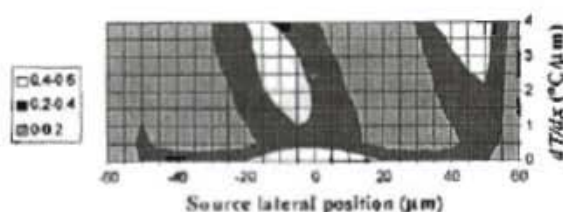

Fig. 7. Normalised output power versus source offset and surface $|dT/dx|$ for 4 constant temperature elements, W_b = 5 μm and L_b = 1 mm

5. BEHAVIOURAL ANALYSIS

A linear temperature gradient gives rise to a linear refractive index region. If a plane wavefront is incident normally on a region in which the refractive index is linearly graded from side to side of the region the plane wavefront will be tilted when it emerges from the region. If the temperature across a width, x, of the region is ΔT, with refractive indices n_1 and n_2 at the edges of the region, the refractive index change from side to side of the region is given by:

$$\Delta n = -0.0003 \Delta T \qquad (3)$$

The amount of tilting of the wavefront depends on how far the beam propagates through the region having the linear temperature gradient. If the distance propagated at the centre of the wavefront is, d, by considering a right angle triangle consisting of the wavefront, the propagation direction and the width normal to the propagation direction we find that the tilt angle is given by:

$$\theta = \tan^{-1}\left(\frac{\Delta n}{x}\frac{d}{(n_1+n_2)/2}\right) \tag{4}$$

Substituting from (3) in (4) yields:

$$\theta = \tan^{-1}\left(\frac{-0.0003}{1.525-0.0003(T_1+T_2)/2}\left(\frac{\Delta T}{x}\right)d\right) \tag{5}$$

Let us now calculate the tilt in the case when the input source is offset by +50 µm, Fig. 5, estimating the temperature gradient in this region to be 0.3 and assuming that the beam propagates 1mm through the linear temperature region. The choice of surface boundary conditions for temperature means that:

$$(T_1+T_2)/2 = 80+\left(\frac{\Delta T}{x}\right)_{surface}\times 20 \tag{6. a}$$

$$(T_1+T_2)/2 = 80-1.5\times 20 = 50 \tag{6. b}$$

Substituting in (5) to obtain the beam steering tilt angle, yields $\theta=3.387°$.

For comparison if we calculate the angle of the taper half-angle, φ, to the propagation direction we obtain:

$$\varphi = \tan^{-1}\left(\frac{(112-25)/2}{1000}\right) = 2.49° \tag{7}$$

Fig. 2(b) shows that without the temperature gradient the incident beam travels along the z direction until it meets the linear taper wall where it reflects so that it makes an angle of $2\varphi=4.98°$ with the z direction. In this arrangement the beam tends to pass to the left of the exit waveguide resulting in poor coupling. However, the effect of the temperature gradient is to tilt this towards the right by θ so that it finally makes an angle of $2\varphi-\theta=1.594°$ with the z direction so the reflected beam travels along the wall of the taper to the exit waveguide resulting in good power coupling.

6. DISCUSSION AND CONCLUSIONS

A thermal gradient of 1.5 °C/µm at the top of the upper cladding layer, $y=+45$ µm, is created by applying a temperature pattern relative to the bottom of the lower cladding layer at $y=-20$ µm, $\Delta T=80, 80, 50, 20$ and 20 °C at five very thin constant temperature stripes centred at $x=-40, -20, 0, 20$ and 40 µm, respectively. This thermal gradient at the surface generates a varying thermal gradient across the centre of the waveguide at $y=+12.5$ µm due to thermal diffusion and the thermal conductivity of the materials of the waveguide layers. The thermal gradient across the centre of the waveguide and within the limits of the input aperture (-56 µm $< x <$ 56 µm) varies from 0.35 at the left edge to -0.16 °C/µm at the right edge, as shown in Fig. 3 (c). This thermal gradient reaches its minimum of -0.37 °C/µm at $x=+4$ µm and reaches its zero value at $x=-29.5$ µm. Its maximum value is reached at the left edge of the input aperture, the zero value is reached between the two left constant temperature elements and the minimum value

is reached under the middle constant temperature element. The thermal gradient decreases continuously from the left edge of the input aperture until just before the right edge of the middle constant temperature element where it starts to increase underneath the two right constant temperature elements until reaching the right edge of the waveguide input aperture. Since the refractive index perturbation is given by, $dn = \Delta T.(dn/dT)$ the negative sign of dn/dT for the waveguide materials causes the temperature rise profile to have the form of an inverted copy of the refractive index perturbation, dn across the centre of the waveguide as shown in Fig. 8.
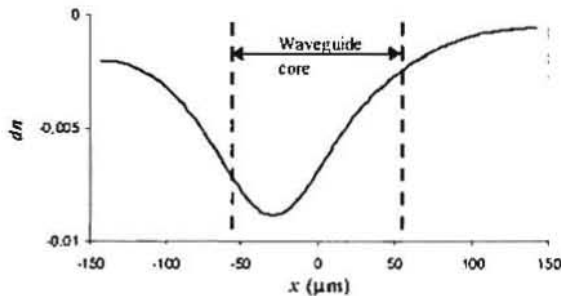

Fig. 8. Refractive index perturbation at $y = +12.5$ μm and $z = 0$ due to five 15 μm wide, 1 mm long constant temperature elements centred at $x = -40, -20, 0, 20$ and 40 μm with $\Delta T = 80, 80, 50, 20$ and 20 °C, respectively

The refractive index across the centre of the waveguide decreases from the left edge of the input aperture until about the left edge of the second left constant temperature element where it starts to increase until the right edge of the input aperture of the waveguide. This explains the optical field propagation shown in Fig. 2

(b) and (c). When the source is offset to $x = +50$ μm with no heat applied the input field does not couple strongly to bound modes [23] since it is very close to the end of the guiding structure giving a normalised output power of 0.22, Fig. 2 (b). When heat is applied the optical power tends to move towards the higher refractive index region at $x \sim +50$ μm near the right edge of the input aperture, shown in Fig. 8 causing the input field to couple into guided modes [23], which leads to an increase in the normalised output power by 2.4 times to 0.52 as shown in Fig. 2 (c). Fig. 5 shows for surface thermal gradients of 1.5 °C/μm the best coupling to guided modes occurs in two regions. The first region is when the ratio of the heater length to the waveguide length is less than 0.45 and source offset is $-23 < x < 20$ μm. The second region is when the ratio of the heater length to the waveguide length is between 0.35 and 1 and source offset is $42 < x < 52$ μm. Fig. 6 shows that increasing the gradient to 2 °C/μm doubles the coupled power compared to the unheated case in the second offset region, and shifts left the coupled power in the first offset region to an offset of $x = -35$ μm. Fig. 7 shows that at low surface thermal gradients of smaller than 0.5 °C/μm stronger coupling to the guided modes occurs in the region $-18 < x < 18$ μm. Surface thermal gradients between 1 and 2.2 °C/μm shift this region to $-15 < x < 0$ μm. Gradients higher than 2.1 °C/μm create another region for good coupling at $35 < x < 52$ μm. In conclusion surface temperature gradients of 0.5 °C/μm cause the taper to lose much of its good lateral offset tolerance. However, as the temperature gradient increases further power coupling is found to improve in two discrete ranges of lateral source offset.

List of Symbols:

n: refractive index

T: temperature

K: thermal conductivity

dn/dT: temperature coefficient of refractive index

φ: half taper angle

W_h: heater width

ΔT: relative temperature

L_h: heater length

u: optical field

k: wavenumber

Q: heat generated per unit volume

θ: tilt angle

d: distance propagated at the centre of wavefront

REFERENCES:

[1] F. Mederer, R. Michalzik, J. Guttmann, H.-P. Huber, B. Lunitz, J. Moisel and D. Wiedenmann, "10 Gb/s data transmission with TO-packaged multimode GaAs VCSELs over 1 m long polymer waveguides for optical backplane applications." *Opt. Comms.*, vol. 206, pp. 309-312, June 2002.

[2] David Israel, Roel Baets, Martin J. Goodwin, Nicola Shaw, Mark D. Salik and Chris J. Groves-Kirkby, "Comparison of Different Polymeric Multimode Star Couplers for Backplane Optical Interconnect." *J. Lightwave Technol.*, vol. 13, No. 6, pp. 1057-1064, June 1995.

[3] Jörg Moisel, "Optical Backplane for Avionic Applications using Polymer Multimode Waveguides," *Proc. of IEEE LEOS Conf.*, Paper WT1, vol. 2, pp. 567-568, 2000.

[4] V. P. Manno, N. R. Kurita and K. Azar, "Experimental Characterization of Board Conduction Effects," *Proc. of the 9th IEEE SEMI-THERM Symp.*, pp. 127-135, Feb. 1993.

[5] H. Shaukatullah and M. Gaynes, "Experimental Determination of Effect of Printed Circuit Card Conductivity on the Thermal Performance of Surface Mount Electronic Packages," *Proc. of the 10th IEEE SEMI-THERM Symp.*, pp. 44-52, Feb. 1994.

[6] V. H. Adams, D. L. Blackburn, Y. K. Joshi, D. W. Berning, "Issues in Validating Package Compact Thermal Models for Natural Convection Cooled Electronic Systems," *IEEE Trans. Comp. Packaging. Manufact. Technol., Part A*, vol. 20, No. 4, pp. 420-431, Dec. 1997.

[7] A. Aranyosi, A. Ortega, R. A. Griffin, S. West and D. R. Edwards, "Compact Thermal Models of Packages Used in Conduction Cooled applications," *IEEE Trans. Comp. and Packaging Technol.*, vol. 23, No. 34, pp. 470-480, Sept. 2000.

[8] H. Nishihara, M. Haruna and T. Suhara, "Thermooptic waveguide devices," in *Optical Integrated Circuits*, pp. 325-330, McGraw-Hill, New York, 1989.

[9] Yasuhiro Hida, Hidekatsu Onose and Saburo Imamura, "Polymer Waveguide Thermooptic Switch with Low Electric Power Consumptions at 1.3 μm," *IEEE Photon. Technol. Lett.*, vol. 5, No. 7, pp. 782-784, July 1993.

[10] W. B. Joyce and B. C. DeLoach, "Alignment of Gaussian Beams," *Appl. Opt.*, vol. 23, No. 23, pp. 4187-4196, Dec. 1984.

[11] Atef M. Rashed and David R. Selviah, "Modelling of Polymer Taper Waveguides for Optical Backplane," *Proc. of Semiconductor and Integrated Optoelecronics Conf.*, Cardiff, Paper 40, April 2004.

[12] Atef M. Rashed, Kevin A. Williams, Peter J. Heard, Richard V. Penty and Ian H. White, "Tapered waveguide with parabolic lens: theory and experiment," *Opt. Eng.*, vol. 41, No. 3, pp. 792-797, March 2003.

[13] M. B. J. Diemeer, J. J. Brons and E. S. Trommel, "Polymeric Optical Waveguide Switch Using the Thermooptic Effect," *J. Lightwave Technol.*, **vol. 7**, No. 3, pp. 449-453, March 1989.

[14] Atef M. Rashed and David R. Selviah, "Source Misalignment in Multimode Polymer Tapered Waveguides for Optical Backplanes," *Opt. Eng.*, vol. 46, No. 1, CJD 015401, Jan. 2007.

[15] W. P. Huang and C. L. Xu, "Simulation of Three-Dimensional Optical Waveguides by a Full-Vector Beam Propagation Method," *IEEE J. Quantum Electron.*, vol. 29, No. 10, pp. 2639-2649, Oct. 1993.

[16] Igor Ilić, Robert Scarmozzino and Richard M. Osgood, Jr., "Investigation of the Padé Approximant-Based Wide-Angle Beam Propagation Method for Accurate Modeling of Waveguiding Circuits," *J. Lightwave Technol.*, vol. 14, No. 12, pp. 2813-2822, Dec. 1996.

[17] Yih-Peng Chiou and Hung-chun Chang, "Analysis of Optical Waveguide Discontinuities Using the Padé Approximants," *IEEE Photon. Technol. Lett.*, vol. 9, No. 7, pp. 964-966, July 1997.

[18] G. R. Hadley, "Transparent boundary condition for the beam propagation method," *IEEE J. Quantum Electron.*, vol. 28, pp. 363-367, 1992.

[19] Igor Ilić, Robert Scarmozzino, Richard M. Osgood, Jr., James T. Yardley, Karl W. Beeson and Michael J. McFarland, "Modeling Multimode-Input Star Couplers in Polymers," *J. Lightwave Technol.*, vol. 12, No. 6, pp. 996-1003, June 1994.

[20] Alberto A. Bilotti, "Static Temperature Distribution in IC Chips with Isothermal Heat Sources," *IEEE Trans. Electron. Devices*, vol. ED-21, No. 3, pp. 217-226, March 1974.

[21] Youngchul Chung and Nadir Dagli, "An Assessment of Finite Difference Beam Propagation Method," *IEEE J. Quantum Electron.*, vol. 26, No. 8, pp. 1335-1339, Aug. 1990.

[22] J. Moisel, H.-P. Huber, J. Guttmann, O. Krumpholz, B. Lunitz, M. Rode and R. Schoedlbauer, "Optical Backplane," *Proc. of ECOC*, Paper We.A.1.5, pp. 254-255, 2001.

[23] Dietrich Marcuse, *"Theory of Dielectric Optical Waveguides,"* Ch. 3, pp. 97-128, Academic Press Inc., San Diego, 1991.